Letter

Spin-Wave Drop Filter Based on Asymmetric Side-Coupled Magnonic Crystals

A. V. Sadovnikov*
Laboratory "Metamaterials," Saratov State University, Saratov 410012, Russia and Kotel'nikov Institute of Radioengineering and Electronics, Russian Academy of Sciences, Moscow 125009, Russia

V. A. Gubanov, S. E. Sheshukova, and Yu. P. Sharaevskii
Laboratory "Metamaterials," Saratov State University, Saratov 410012, Russia

S. A. Nikitov
Laboratory "Metamaterials," Saratov State University, Saratov 410012, Russia and Kotel'nikov Institute of Radioengineering and Electronics, Russian Academy of Science, Moscow 125009, Russia

(Received 9 January 2018; published 23 May 2018)

Space-resolved Brillouin light-scattering spectroscopy and micromagnetic simulations are used to study the propagation of magnetostatic spin waves across nonidentical magnonic crystals within close proximity. We show that the characteristics of spin-wave modes in such structure depends on the geometry of adjacent magnonic crystals. In particular, our results demonstrate that the efficient spin-wave coupling at the frequency of the magnonic forbidden gap can be achieved, enabling the spin-wave power drop between asymmetric magnonic crystals. We demonstrate, that the combination of spatial-filtering features and the spin-wave coupling in the adjacent magnonic crystals leads to the realization of the frequency-selective magnonic drop filter which is expected to offer new functionalities for spin-wave demultiplexing applications within the complex magnonic circuitry.

DOI: 10.1103/PhysRevApplied.9.051002

In recent years, much research has been directed towards the use of spin waves (SWs) for signal processing at microwave and subterahertz frequencies [1] due to the possibility to carry the information signal without the transmission of a charge current (see Ref. [2] and references therein). Magnonic crystals (MCs) have attracted significant attention due to their wide range of applications and numerous ways to fabrication [3–9]. MCs are used in linear and nonlinear magnonics as a building block of magnonic networks [10–17]. In the majority of the previously realized devices the MCs have been used as the high-Q tunable rejection filter due to the most important features of the MCs—the magnonic forbidden (rejection) band or magnonic band gap in the spin-wave spectra [3]. However, the possible use of the magnonic forbidden band to fabricate the drop filters in magnonic integrated circuits can extend the application of MCs, in particular, for the magnonic logic [18]. The more complex the magnonic network, the more nodes are needed, the more interjunctions between the magnonic functional blocks are required. The connection of functional magnonic units in a magnon circuit is an undisputed challenge. The recently demonstrated phenomenon of propagating spin-wave coupling [19–21] has inspired a lot of interest due to the possible applications for controlling the spin-wave propagation [22,23] and fabrication of micro- and nanodevices based on low-loss insulating magnetic materials [24]. The magnonic directional coupler (MDC) based on adjacent magnetic stripes has the frequency-selective features due to the periodic power transfer from one waveguide to the other at a distance L as a result of the symmetrical and antisymmetrical spin-wave mode interference [21]. Thus, the input power can be divided between the output ports with the frequency-dependent ratio due to the frequency dependence of the coupling length $L(f)$ [21,23]. The major limitation of the conventional MDCs is the relatively high frequency range of effective spin-wave coupling [21,23,25–28]. The standard strategy to reduce the frequency range of effective power transmission between the magnetic stripes and, thus, to enhance the wavelength selectivity consists of increasing the value of dL/df. For a typical magnonic coupler this can be achieved by the increase of spin-wave wave numbers [19,21,23,24]. However, the latter leads to the decrease of the group velocity and, thus, to the decrease of the propagation length of the dipolar SWs [29,30]. Therefore, the transmission of the spin-wave signal through the MDC is significantly reduced.

*sadovnikovav@gmail.com

Here, we present an alternative way to enhance the frequency selectivity by the use of the concept of side-coupled MCs. Two magnonic crystals of different width, period, or saturation magnetization placed in proximity can be treated as side-coupled asymmetric MCs. In this structure, the spin waves have nonequal propagation constants and, thus, the phase-matching condition is violated. While phase mismatch might seem on the surface to decrease the coupling efficiency, the unusual increase of the spin-wave coupling can be observed at the frequencies in the vicinity of the magnonic band gap. This idea can underpin the experimental and theoretical studies regarding the side-coupled magnonic crystals [31], which can also act as frequency-selective multiplexers [23,32–34].

In this Letter, we report the experimental observation of the spin-wave coupling in the asymmetric adjacent magnonic crystals based on multimode yttrium-iron-garnet (YIG) waveguides. We show that the combination of frequency- and spatial-filtering features of the MC and spin-wave coupling in the adjacent magnetic waveguide leads to the realization of the magnonic drop filter. We also identify the mechanism of the efficient spin-wave power transmission between the magnonic crystals. As a major result, we demonstrate by the means of the space-resolved Brillouin light-scattering (BLS) technique, that nonidentical MCs within close proximity demonstrate the efficient spin-wave coupling at the frequency of the magnonic forbidden gap of one of the MCs. Thus, MCs can be used not only to achieve the spatial and frequency filtering of the spin-wave signal but also to provide the phase condition with an efficient spin-wave power transfer from the input to the drop port of the magnonic coupler.

The schematic of the experimental layout is sketched in Fig. 1(a). The coupled magnetic stripes of width $w_1 = 500$ μm (MC1) and $w_2 = 200$ μm (MC2) with a $d = 30$ μm edge-to-edge spacing are fabricated from $t = 10$ μm-thick monocrystalline ferrimagnetic YIG film with a saturation magnetization of $M_0 = 139$ G on the 500-μm-thick gallium-gadolinium-garnet substrate using the precise laser ablation technique.

The periodic sequences of the grooves of $d_g = 1.1$ μm depth with the period of $D = 200$ μm are fabricated on the surface of the both YIG stripes using the precise ion-beam etching. Both MCs had 25 periods along the coupling region with the length of $L_c = 5$ mm. As it is shown in Fig. 1(a), we denote the output area of the coupling region inside MC1 and MC2 as a port P_1 and P_2, respectively.

The excitation of spin waves in MC1 is performed by utilizing the 50-Ω matched microstrip transmission line with the gold microwave transducers of 40-μm width. The input and output transducers are attached to MC1 at a distance of 8 mm between each other. The uniform static magnetic field $H_0 = 1300$ Oe is applied in the plane of the structure along the z direction for the effective excitation of the magnetostatic surface waves [35,36].

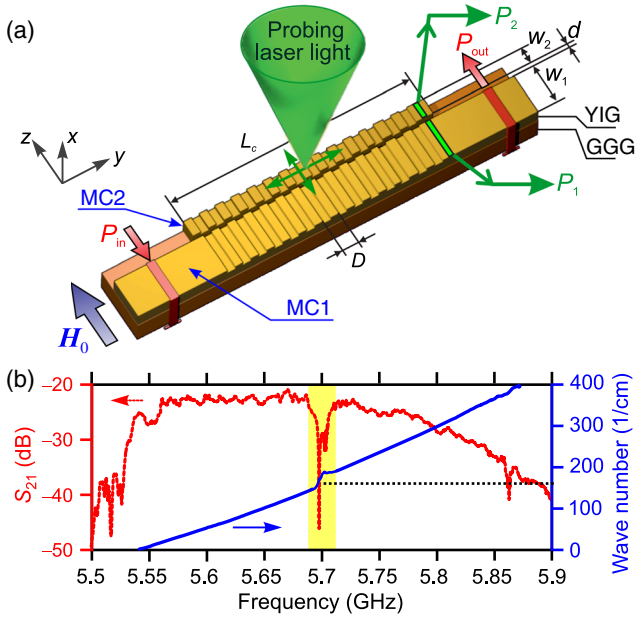

FIG. 1. (a) Schematic of the experiment: nonidentical side-coupled magnonic crystals of period D; microwave transducers at input and output to perform the microwave experiment by the means of VNA; probing laser light for space-resolved BLS measurement. (b) Spin-wave transmission (red curve) and dispersion (blue curve) characteristics measured by VNA at MC1. The value of the Bragg wave number is denoted with the horizontal dashed line.

We first investigate the spin-wave transmission response for the fabricated device using the microwave spectroscopy technique based on the E8362C PNA vector network analyzer (VNA). The solid red curve in Fig. 1(b) shows the measured absolute value of S_{21}. The input power of the microwave signal is of −10 dBm in order to avoid nonlinear effects at this frequency range [29,31]. A well-pronounced rejection band with the width of $\Delta f_B = 0.03$ GHz at the level of −30 dB is clearly observed at the frequency of $f_1 = 5.7$ GHz. To verify that the frequency f_1 is the center frequency of the magnonic forbidden gap we measure the phase-frequency response and acquire the dispersion characteristics denoted with the blue dashed curve in Fig. 1(b). As it is seen from Fig. 1(b), the frequency f_1 corresponds to the Bragg wave number $k_y = k_B = \pi/D = 157$ cm^{-1}, and thus to the central frequency of the first forbidden zone (magnonic band gap).

In the following, we demonstrate the spin-wave coupling by means of spatially resolved BLS spectroscopy in the quasibackscattering geometry. We perform the scanning with the probing laser light with the wavelength of 532 nm of the 5×0.73 mm^2 area on the surface of the MC1 and MC2. The intensity of the resulting BLS signal is proportional to the dynamic magnetization squared at the position of the probing spot. The two-dimensional spatial maps of the spin-wave intensity with the spatial resolution of 25 μm

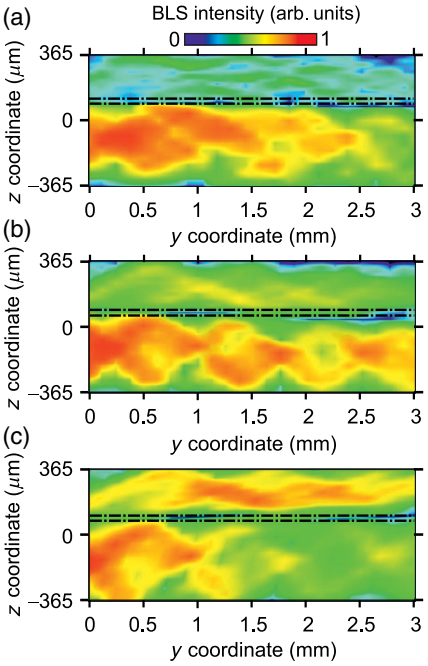

FIG. 2. (a) Normalized color-coded two-dimensional BLS intensity map of magnetization squared demonstrating the spin-wave propagation at the excitation frequencies of $f = 5.65$ GHz (a), $f = 5.68$ GHz (b), and $f = 5.7$ GHz (c).

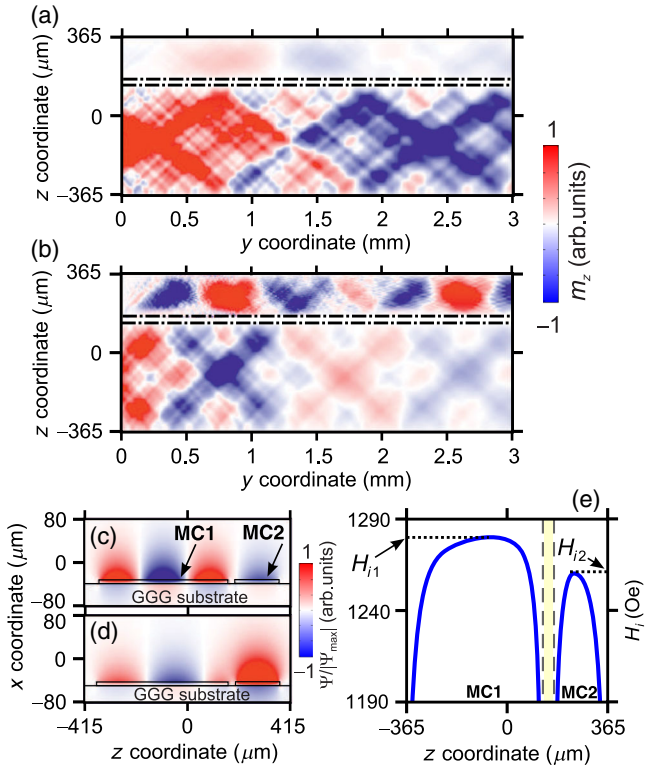

FIG. 3. The results of micromagnetic simulation: snapshot of m_z component in the adjacent MCs at $f = 5.68$ GHz (a) and $f = f_1 = 5.7$ GHz (b); (c) and (d) show profiles of the quasisymmetrical and quasiantisymmetrical modes; (e) shows the internal magnetic field profile in both MCs.

are shown in Fig. 2. The reason for the absence of the power exchange between the MCs at the frequency below the f_1 [see Figs. 2(a) and 2(b)] is the low spin-wave coupling efficiency due to wave-number mismatch between adjacent asymmetric magnonic crystals (MC1 and MC2). However, as it is shown in Fig. 2(c) at the frequency of the magnonic band gap f_1 one can observe the strong spin-wave coupling between the asymmetric MCs. The spin-wave signal drops from the input of MC1 at the frequency of f_1 and is transmitted to the output port P_2 of MC2.

Next, to support these findings, we perform the micromagnetic study of spin-wave propagation along the side-coupled waveguides (see Fig. 3). In spite of the case of the backward volume magnetostatic spin-wave coupling [37], where the analytical expressions of the coupling coefficients and spin-wave dispersion can be obtained, only the straightforward micromagnetic calculation of the surface spin-wave coupling is possible, due to highly nonuniform internal magnetic field profiles inside the adjacent magnonic stripes. Therefore, we use the Object-Oriented Micro- Magnetic Framework (OOMMF) [38] to perform the numerical solution of the Landau-Lifshitz equation for the dynamics of the magnetization [39]. The volume of the simulation area is $(3000 \times 730 \times 10)\ \mu\text{m}^3$, the size of the mesh cell is $(0.1 \times 0.1 \times 1)\ \mu\text{m}^3$. First, we perform the static simulation to obtain the ground magnetic state of coupled MCs. Therefore, we define the internal magnetic field profile $H_i(z)$ [see Fig. 3(e)]. Next, the SWs are excited in the vicinity of the left edge of MC1 by a local magnetic field of harmonic temporal profile. Figure 3(a) demonstrates the dynamic out-of-plane component of magnetization m_z after a lapse of 200 ns from the onset of the excitation at the frequency of 5.1 GHz. Because of the effective excitation of the first and third transverse modes [36,40], the multimode spin-wave propagation is observed in MC1 and the weak coupling with MC2 is also seen. At the frequency of f_1 the SW drops to the output of MC2.

The observed signal drop can be qualitatively explained taking into account the two mechanisms which can lead to the frequency shift of the magnonic band gap in MC1 and MC2. First, we need to take into account the redshift of the lower cutoff frequency of the first transverse mode in the YIG stripe of finite width [40]. Figure 4(a) shows the dispersion of the first, second, and third transverse mode for the stripe of width w_1 (blue solid curve) and w_2 (green dashed curve). Second, it should be noted that in the adjacent magnonic stripes the internal magnetic field H_i is reduced due to the shape anisotropy. The frequency of ferromagnetic resonance for the in-plane magnetized stripe [41] can be defined as $f_{1,2} = \gamma/(2\pi)\sqrt{H_{i1,2}(H_{i1,2} + 4\pi M_0)}$, where $\gamma/2\pi = 2.8$ MHz/Oe is the gyromagnetic ratio for YIG, $H_{i1} = 1179$ Oe and $H_{i2} = 1162$ Oe are the values of internal magnetic field in the center of the stripe of widths

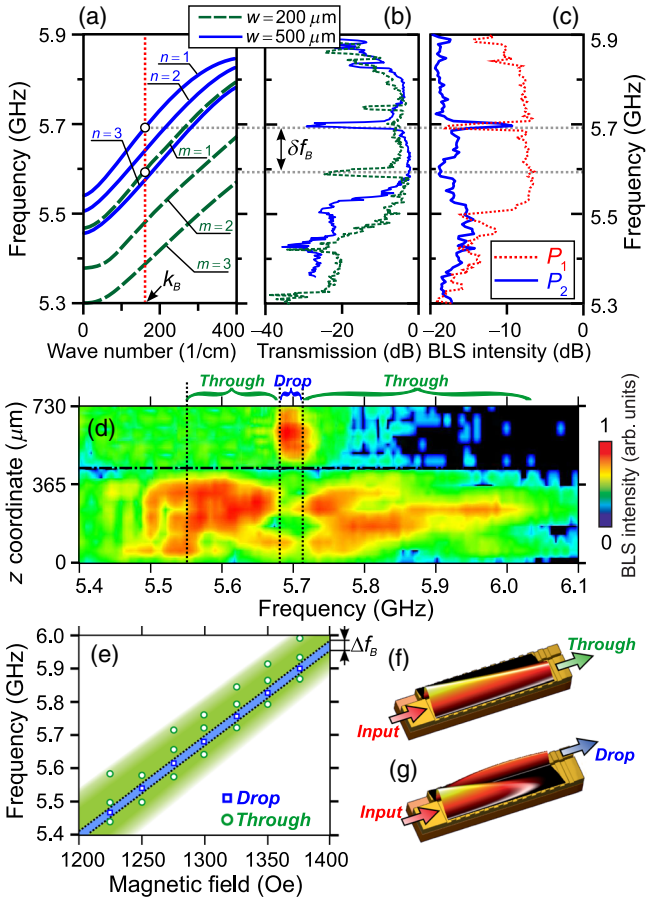

FIG. 4. (a) Dispersion of the spin waves in the magnonic stripes of width 200 μm (dashed green curves) and 500 μm (solid blue curves). (b) Spin-wave transmission response in the separate magnonic crystal of the widths of 200 μm (dashed green curves) and 500 μm (solid blue curves). Horizontal dotted lines show the frequencies of magnonic forbidden gap. The frequency mismatch of the forbidden-gap position is denoted by δf_B. (c) Frequency dependence of BLS intensity at the output position of MC1 (P_1, red dashed curve) and MC2 (P_2, blue solid curve). (d) Frequency dependence of BLS signal across the z coordinate at the output position of magnonic crystals. (e) Magnetic field tunability of the drop filter. The shaded green and blue colors denote the numerical simulation results; BLS data: open circles demonstrate the "through" regime (f) and open squares—the "drop" regime (g).

w_1 and w_2, respectively, estimated from the micromagnetic simulation [38] [see Fig. 3(e)].

One should note from Fig. 4(a), that the dispersion branch of the first transverse mode in the stripe of width w_2 almost coincides with the dispersion branch of the third mode of the stripe of w_1. This leads to the effective coupling of the third mode of MC1 and the first mode of MC1. The quantitative explanation of this effect can be provided via the calculation of eigenmode spectra of the side-coupled magnonic stripe of a finite width. When two identical parallel magnetic stripes are brought in proximity, the SWs are coupled by the dipolar field and the spin-wave dispersion branch of an isolated waveguide is split into symmetrical and antisymmetrical spin-wave modes. In the case of nonidentical magnonic stripes the eigenmode spectrum consists of the quasisymmetrical (QS) and quasiantisymmetrical (QAS) modes. By the means of the finite-element method (FEM) [21,42] we calculate the eigenmode spectra and mode profiles of the laterally asymmetric parallel magnetic stripes with the nonuniform static internal magnetic field. These calculations show that the effective coupling is possible between the third transverse mode in MC1 and first mode in MC2. Figures 3(c) and 3(d) show the field profile of the QS and QAS modes, respectively. The interference of these modes defines the spatial spin-wave intensity pattern in asymmetrical side-coupled magnonic stripes. We have to emphasize that the spin-wave propagation constants mismatch in both MCs allow one the use of the weak coupling approximation to describe the characteristics of coupled spin waves. Thus, the spin-wave dynamics can be described by the means of the solution of coupled mode equations [24] taking into account the results of FEM calculation, in particular, the wave numbers of the QS and QAS modes. Thus, there are two mechanisms leading to the energy transfer between the nonidentical MCs. The first is the multimode coupling and the second is the spin-wave forbidden-frequencies mismatch due to the shape anisotropy of MCs.

The calculated spin-wave transmission response in the separate MC of widths w_1 and w_2 is denoted with blue-solid and green-dashed curves in Fig. 4(b), respectively. The frequency positions of the first magnonic forbidden zone in these MCs are noticeably different from each other, enabling the signal propagation along MC2 with the frequency in the vicinity of the band gap of MC1. In other words, the mismatch between the frequencies of the magnonic band gaps of MC1 and MC2 opens the possibility to signal drop from the input of MC1 to the output of MC2 (drop port) at the frequencies inside the magnetic forbidden zone of MC1.

The frequency dependence of the BLS signal at the ports P_1 and P_2 reveals the well-defined peak at the frequency of f_1 in the drop port. The width of this peak is about $\Delta f = 15$ MHz, which corresponds to the width of the magnonic band gap (at 3 dB level). This value is in good agreement with the theoretical value of the forbidden frequency gap width of single MC [43]: $\Delta f = (\gamma 4\pi M_0)^2(2\pi/D)(d_g/t)\exp[-\pi t/D] \approx 12.4$ MHz. Thus, the band-gap-induced transmission band is at least 5 times narrower than the transmission band in the conventional magnonic coupler [21,23,24]. The drop efficiency reads as $T_{21}(f) = 10\log[P_2(f)/P_1(f)]$ and defines the ratio between the spin-wave power transmitted in drop port P_2 from the MC1. The maximum value of $T_{21} = 8$ dB is reached at the frequency of f_1.

Figure 4(d) shows the frequency dependence of the intensity of the BLS signal $I(y,z)$ at the y position, which corresponds to the position of ports P_1 and P_2. At the frequency range in the vicinity of f_1 the proposed coupler operates in the "drop regime" when the signal attenuation in port P_1 is visible and the increase of the spin-wave intensity in port P_2 is clearly observable. Below and above the frequency range $f_1 - \Delta f/2 < f < f_1 + \Delta f/2$ the "through regime" is realized, when the spin-wave power propagates along the MC1 without coupling to MC2.

One of the most important features of the proposed magnonic drop filter is to be adjustable. By the variation of both the value and angle of the bias magnetic field the frequency position of the magnonic band gap and the frequency region of the transverse modes coupling can be adjusted [21,37]. Thus, the drop frequency can be tuned in a wide operation range, which is shown in Fig. 4(e).

In conclusion, we systematically investigate the spin-wave coupling in the nonidentical (asymmetrical) adjacent magnonic crystals. We demonstrate that the spin-wave coupling efficiency in the waveguiding nonidentical periodical structure within close proximity can be significantly increased in the frequency range of the magnonic band gap. In spite of the absence of full energy transfer between the nonidentical magnonic crystals, the proposed structure demonstrates the narrow frequency range of the efficient spin-wave signal drop between the magnonic crystals. We show that the intermodal coupling and the frequency shift of magnonic band gaps in adjacent structures is responsible for the observed narrow frequency range of the spin-wave power transmission between the magnonic crystals. Using the asymmetric side-coupled magnonic crystals we fabricate the drop filter, which is the base for a variety of magnonic switching and routing devices.

The structure fabrication and BLS measurement were supported by the grant from RSF (No. 16-19-10283), the microwave experiments were supported by RSF (No. 14-19-00760), micromagnetic simulations were supported by RFBR (18-57-76001). A. V. S. and S. E. S. acknowledge support from the Scholarship of the President of RF (No. SP-2819.2018.5) and the Grant of the President of RF (No. MK-3650.2018.9).

[1] S. O. Demokritov, *Spin Wave Confinement: Propagating Waves*, 2nd ed. (Pan Stanford Publishing Pte. Ltd, Singapore, 2017).

[2] D. Sander, S. O. Valenzuela, D. Makarov, C. H. Marrows, E. E. Fullerton, P. Fischer, J. McCord, P. Vavassori, S. Mangin, P. Pirro, B. Hillebrands, A. D. Kent, T. Jungwirth, O. Gutfleisch, C. G. Kim, and A. Berger, The 2017 magnetism roadmap, J. Phys. D **50**, 363001 (2017).

[3] S. A. Nikitov, P. Tailhades, and C. S. Tsai, Spin waves in periodic magnetic structures magnonic crystals, J. Magn. Magn. Mater. **236**, 320 (2001).

[4] A. V. Chumak, T. Neumann, A. A. Serga, B. Hillebrands, and M. P. Kostylev, A current-controlled, dynamic magnonic crystal, J. Phys. D **42**, 205005 (2009).

[5] A. V. Chumak, V. I. Vasyuchka, A. A. Serga, and B. Hillebrands, Magnon spintronics, Nat. Phys. **11**, 453 (2015).

[6] S. E. Sheshukova, E. N. Beginin, A. V. Sadovnikov, Yu. P. Sharaevsky, and S. A. Nikitov, Multimode propagation of magnetostatic waves in a width-modulated yttrium-iron-garnet waveguide, IEEE Magn. Lett. **5**, 1 (2014).

[7] G. Gubbiotti, S. Tacchi, M. Madami, G. Carlotti, A. O. Adeyeye, and M. Kostylev, Brillouin light scattering studies of planar metallic magnonic crystals, J. Phys. D **43**, 264003 (2010).

[8] Dirk Grundler, Reconfigurable magnonics heats up, Nat. Phys. **11**, 438 (2015).

[9] A. V. Chumak, A. A. Serga, and B. Hillebrands, Magnonic crystals for data processing, J. Phys. D **50**, 244001 (2017).

[10] V. V. Kruglyak, S. O. Demokritov, and D. Grundler, Magnonics, J. Phys. D **43**, 264001 (2010).

[11] S. Neusser and D. Grundler, Magnonics: Spin waves on the nanoscale, Adv. Mater. **21**, 2927 (2009).

[12] A. V. Chumak, A. A. Serga, and B. Hillebrands, Magnon transistor for all-magnon data processing, Nat. Commun. **5**, 4700 (2014).

[13] A. V. Sadovnikov, S. Davies, S. V. Grishin, V. V. Kruglyak, D. V. Romanenko, Yu. P. Sharaevskii, and S. A. Nikitov, Magnonic beam splitter: The building block of parallel magnonic circuitry, Appl. Phys. Lett. **106**, 192406 (2015).

[14] C. S. Davies, A. Francis, A. V. Sadovnikov, S. V. Chertopalov, M. T. Bryan, S. V. Grishin, D. A. Allwood, Y. P. Sharaevskii, S. A. Nikitov, and V. V. Kruglyak, Towards graded-index magnonics: Steering spin waves in magnonic networks, Phys. Rev. B **92**, 020408 (2015).

[15] V. E. Demidov, S. Urazhdin, A. Zholud, A. V. Sadovnikov, A. N. Slavin, and S. O. Demokritov, Spin-current nano-oscillator based on nonlocal spin injection, Sci. Rep. **5**, 8578 (2015).

[16] V. E. Demidov, S. Urazhdin, A. Zholud, A. V. Sadovnikov, and S. O. Demokritov, Dipolar field-induced spin-wave waveguides for spin-torque magnonics, Appl. Phys. Lett. **106**, 022403 (2015).

[17] A. V. Sadovnikov, E. N. Beginin, S. A. Odincov, S. E. Sheshukova, Yu. P. Sharaevskii, A. I. Stognij, and S. A. Nikitov, Frequency selective tunable spin wave channeling in the magnonic network, Appl. Phys. Lett. **108**, 172411 (2016).

[18] Alexander Khitun, Multi-frequency magnonic logic circuits for parallel data processing, J. Appl. Phys. **111**, 054307 (2012).

[19] A. Yu. Annenkov and S. V. Gerus, Propagation of magnetostatic waves in two coupled channels created by a magnetic field, J. Commun. Technol. Electron. **41**, 196 (1996).

[20] M. P. Kostylev, G. Gubbiotti, J. G. Hu, G. Carlotti, T. Ono, and R. L. Stamps, Dipole-exchange propagating spin-wave modes in metallic ferromagnetic stripes, Phys. Rev. B **76**, 054422 (2007).

[21] A. V. Sadovnikov, E. N. Beginin, S. E. Sheshukova, D. V. Romanenko, Yu. P. Sharaevskii, and S. A. Nikitov,

Directional multimode coupler for planar magnonics: Side-coupled magnetic stripes, Appl. Phys. Lett. **107**, 202405 (2015).

[22] A. V. Sadovnikov, A. A. Grachev, E. N. Beginin, S. E. Sheshukova, Yu. P. Sharaevskii, and S. A. Nikitov, Voltage-Controlled Spin-Wave Coupling in Adjacent Ferromagnetic-Ferroelectric Heterostructures, Phys. Rev. Applied **7**, 014013 (2017).

[23] Qi Wang, Philipp Pirro, Roman Verba, Andrei Slavin, Burkard Hillebrands, and Andrii V. Chumak, Reconfigurable nano-scale spin-wave directional coupler, Sci. Adv. **4**, e1701517 (2018).

[24] A. V. Sadovnikov, S. A. Odintsov, E. N. Beginin, S. E. Sheshukova, Yu. P. Sharaevskii, and S. A. Nikitov, Toward nonlinear magnonics: Intensity-dependent spin-wave switching in insulating side-coupled magnetic stripes, Phys. Rev. B **96**, 144428 (2017).

[25] A. K. Ganguly and C. Vittoria, Magnetostatic wave propagation in double layers of magnetically anisotropic slabs, J. Appl. Phys. **45**, 4665 (1974).

[26] A. K. Ganguly and D. C. Webb, Radiation resistance of microstrip excited magnetostatic surface waves, in *Proceedings of the Microwave Symposium, 1975 IEEE-MTT-S International* (IEEE, 1975).

[27] H. Sasaki and N. Mikoshiba, Directional coupling of magnetostatic surface waves in layered magnetic thin films, Electron. Lett. **15**, 172 (1979).

[28] H. Sasaki and N. Mikoshiba, Directional coupling of magnetostatic surface waves in a layered structure of YIG films, J. Appl. Phys. **52**, 3546 (1981).

[29] A. G. Gurevich and G. A. Melkov, *Magnetization Oscillations and Waves* (CRC-Press, London, New York, 1996).

[30] D. D. Stancil and A. Prabhakar, *Spin Waves: Theory and Applications* (Springer, New York, 2009).

[31] A. V. Sadovnikov, E. N. Beginin, M. A. Morozova, Yu. P. Sharaevskii, S. V. Grishin, S. E. Sheshukova, and S. A. Nikitov, Nonlinear spin wave coupling in adjacent magnonic crystals, Appl. Phys. Lett. **109**, 042407 (2016).

[32] K. Vogt, F. Y. Fradin, J. E. Pearson, T. Sebastian, S. D. Bader, B. Hillebrands, A. Hoffmann, and H. Schultheiss, Realization of a spin-wave multiplexer, Nat. Commun. **5**, 3727 (2014).

[33] C. S. Davies, A. V. Sadovnikov, S. V. Grishin, Y. P. Sharaevsky, S. A. Nikitov, and V. V. Kruglyak, Field-controlled phase-rectified magnonic multiplexer, IEEE Trans. Magn. **51**, 1 (2015).

[34] F. Heussner, A. A. Serga, T. Brächer, B. Hillebrands, and P. Pirro, A switchable spin-wave signal splitter for magnonic networks, Appl. Phys. Lett. **111**, 122401 (2017).

[35] R. W. Damon and J. Eschbach, Magnetostatic modes of a ferromagnet slab, J. Phys. Chem. Solids **19**, 308 (1961).

[36] S. N. Bajpai, Excitation of magnetostatic surface waves: Effect of finite sample width, J. Appl. Phys. **58**, 910 (1985).

[37] A. V. Sadovnikov, S. A. Odintsov, E. N. Beginin, S. E. Sheshukova, Yu. P. Sharaevskii, and S. A. Nikitov, Spin-wave switching in the side-coupled magnonic stripes, IEEE Trans. Magn. **53**, 1 (2017).

[38] M. J. Donahue and D. G. Porter, *OOMMF Users Guide, 1.0* (NISITR, Gaithersburg, MD, 1999).

[39] L. Landau and E. Lifshitz, On the theory of the dispersion of magnetic permeability in ferromagnetic bodies, Phys. Z. Sowjetunion **8**, 153 (1935).

[40] T. W. O'Keefe and R. W. Patterson, Magnetostatic surface-wave propagation in finite samples, J. Appl. Phys. **49**, 4886 (1978).

[41] C. Kittel, Ferromagnetic resonance, J. Phys. Radium **12**, 291 (1951).

[42] M. Koshiba, K. Hayata, and M. Suzuki, Finite-element solution of anisotropic waveguides with arbitrary tensor permittivity, J. Lightwave Technol. **4**, 121 (1986).

[43] Yu. Gulyaev, S. Nikitov, and V. Plesskii, Reflection of surface magnetostatic waves from periodically nonuniform ferrite surface, Radiotekh. Elektron. **26**, 2282 (1981).